



## Dynamics of Supramolecular Self-Healing Recovery in Extension

Hinton, Zachary R.; Shabbir, Aamir; Alvarez, Nicolas J.

*Published in:*  
Macromolecules

*Link to article, DOI:*  
[10.1021/acs.macromol.8b02423](https://doi.org/10.1021/acs.macromol.8b02423)

*Publication date:*  
2019

*Document Version*  
Peer reviewed version

[Link back to DTU Orbit](#)

*Citation (APA):*  
Hinton, Z. R., Shabbir, A., & Alvarez, N. J. (2019). Dynamics of Supramolecular Self-Healing Recovery in Extension. *Macromolecules*, 52(6), 2231-2242. <https://doi.org/10.1021/acs.macromol.8b02423>

---

### General rights

Copyright and moral rights for the publications made accessible in the public portal are retained by the authors and/or other copyright owners and it is a condition of accessing publications that users recognise and abide by the legal requirements associated with these rights.

- Users may download and print one copy of any publication from the public portal for the purpose of private study or research.
- You may not further distribute the material or use it for any profit-making activity or commercial gain
- You may freely distribute the URL identifying the publication in the public portal

If you believe that this document breaches copyright please contact us providing details, and we will remove access to the work immediately and investigate your claim.

# The Dynamics of Supramolecular Self-Healing Recovery in Extension

Zachary R. Hinton,<sup>†</sup> Aamir Shabbir,<sup>‡,¶</sup> and Nicolas J. Alvarez<sup>\*,†</sup>

<sup>†</sup>*Department of Chemical and Biological Engineering, Drexel University, Philadelphia, PA  
19104, USA*

<sup>‡</sup>*Department of Chemical Engineering, Technical University of Denmark, 2800 Kgs.  
Lyngby, Denmark*

<sup>¶</sup>*Current address: Coloplast, Hulebaek, Denmark*

## Abstract

Self-healing materials are prized for their ability to recover mechanical properties after damage. Supramolecular polymer networks have been demonstrated to have the ability to recover without the need for extraneous material components or the use of external stimuli. However, there is little quantitative measure of self-healing dynamics and recovery. In this work, we use extensional rheology measurements in creep and constant rate of extension to quantify the dynamics of the recovery process. Using a model entangled network, poly(*n*-butyl acrylate), with varying number of poly(acrylic acid) hydrogen bonding groups, and an unentangled associating network, poly(methoxyethyl acrylate) with 6-methyl-2-ureido-4[1H]-pyrimidone-bearing (UPy) methacrylate groups, we quantify the effect of network architecture on the recovery process. We experimentally confirm that the waiting time ( $\tau_W$ ) controls the state of the network at the interface, largely affecting the magnitude and timescale of recovery of the network, subject to the number of available free associations. Recovery of the network is also strongly dependent on the healing time ( $\tau_H$ ) and network architecture.

For entangled polymers, the recovery process is sequential, with chain dynamics dominating at low healing times ( $\tau_H$ ) followed by recovery of associations. For unentangled polymers, recovery is controlled by association dynamics alone. The definition of recovery is not trivial and depends dramatically on the network architecture, applied kinematic flow (or  $Wi$ ),  $\tau_H$ , and  $\tau_W$ . We construct a framework for future rheological measurements of the recovery dynamics of self-healing soft materials which highlights the importance of experimental protocol when reporting recovery properties.

## Introduction

Supramolecular networks are a diverse class of polymeric materials which are crosslinked via secondary interactions (often referred to as stickers) such as hydrogen-bonding,<sup>1-4</sup> ionic<sup>5,6</sup> / metallic<sup>7,8</sup> interactions, and steric assemblies<sup>9,10</sup> (e.g.  $\pi$ - $\pi$  stacking). These networks are highly promising as autonomic ‘self-healing’ materials, i.e. materials which, after damage, are able to partially or fully recover mechanical strength without outside intervention.<sup>11-16</sup> While many traditional self-healing polymers require the introduction of a reactive species to recover,<sup>17-24</sup> some self-healing polymers recover intrinsically via polymer dynamics.<sup>11</sup> Although in some applications these dynamics are enhanced using heat<sup>25,26</sup> or solvent,<sup>27,28</sup> materials that are both autonomic and intrinsic are highly desirable.

Previous measures of supramolecular polymer dynamics have shown that their rheological response is highly dependent on: the number, strength, and distribution of associating groups along the polymer backbone.<sup>29-33</sup> For all self-associating polymers, the linear viscoelastic response is highly affected at long times (low frequency) due to the long lifetimes (high bonding energy) of associating groups. In non-linear extensional rheology, associating polymers act as crosslinked networks with increased strain hardening effects at very low strain-rates. Surprisingly in entangled polymer melts, the hydrogen bonds have little effect on polymer dynamics at times faster than the disengagement time.<sup>29</sup> It is well understood that associating chemical groups delay diffusion and reptation of chains.<sup>34-36</sup> However, there

is a complex relationship between competing timescales that are not well understood. In this work, we correlate measured association dynamics with well-defined timescales to determine the mechanisms and extent of recovery expected for associating polymers with and without entanglements.

When a supramolecular network is fractured, a non-equilibrium state of stretched and dangling chains is created. When the fractured surfaces are put into contact, both entanglements and associations reform across the interface. Given sufficient time the interface is said to achieve a steady state recovery of the material. The degree of recovery in associating polymers is governed by two primary timescales: the waiting time ( $\tau_W$ ) and the healing time ( $\tau_H$ ). The waiting time occurs between the time of damage and the recovery stage. During the waiting time, the two halves of the material evolve toward separate states which may differ from that of the undamaged material.<sup>13</sup> When the two halves are recontacted, the healing time begins, during which the material moves toward its original state, recovering some degree of its undamaged mechanical properties. The exact mechanism by which entanglements and associations reform and to what degree the steady state recovery approximates equilibrium is of considerable importance when designing superior materials with self-healing characteristics.

A comprehensive theoretical framework for self-healing recovery of supramolecular polymers was developed by Rubinstein, Leibler, and co-workers.<sup>13</sup> In this model, recovery of the network is defined in terms of the number of bridges made across the fractured interface, which depends on: (i) network architecture, (ii)  $\tau_W$ , and (iii)  $\tau_H$ . The authors conclude that the dynamics of recovery are uniquely determined by the value of  $\tau_W$ , since it defines the state of the damaged surfaces before recovery. For high bond strength,  $\epsilon$ , defined as,  $\epsilon \gg 2k_B T \ln(N)$ , where  $N$  is the number of monomers in a sticky segment, Rubinstein and co-workers define four recovery regimes that are bounded by the relative value of  $\tau_W$  to:  $\tau_R$ , the Rouse time of a dangling chain,  $\tau_b$ , the average association lifetime,  $\tau_{eq}$ , the equilibration time of open stickers, and  $\tau_{adh}$ , the time to reach the undamaged state. For  $\tau_W < \tau_R$ ,

dangling chains do not have sufficient time to diffuse away from the fractured surface and therefore associations readily recover to a sub-equilibrium state. For  $\tau_H < \tau_R$ , the degree of recovery is proportional to  $\tau_H$  and constant for  $\tau_R < \tau_H < \tau_{eq}$ . For  $\tau_R < \tau_W < \tau_b$ , dangling chains diffuse away from the fractured surface and paired associations do not have sufficient time to exchange partners. This regime is characterized by very little recovery with increasing  $\tau_H$  until  $\tau_H = \tau_{eq}$ . For  $\tau_b < \tau_W < \tau_{eq}$ , new dangling chains are available but are scavenged by associating groups within the respective network and are not available for bridging at the fractured surface. This leads to even slower recovery with  $\tau_H$  until  $\tau_H = \tau_{eq}$ . Lastly, for  $\tau_{eq} < \tau_W < \tau_{adh}$ , recovery is increasing with  $\tau_H$  and results in the lowest degree of recovery for  $\tau_H < \tau_{eq}$  compared to lower values of  $\tau_W$ . For  $\tau_H \gg \tau_{eq}$ , the number of bridges is the same for all values of  $\tau_W$ . This model has not yet been validated experimentally. In this work, we use the model's simple scaling arguments to quantify critical timescales which give important insight into both recovery dynamics and the role of network architecture on self-healing behavior.

Little experimental data is available to validate the fundamental phenomena responsible for mechanical recovery of supramolecular polymers. Moreover, it is not clear how best to measure self-healing recovery of viscoelastic materials. The properties of some self-healing polymers allow for solid mechanical testing,<sup>12,14</sup> however, viscoelastic materials display more complex rheology which requires more robust characterization techniques. Various measures of recovery have been made using shear rheology of entangled polymers,<sup>37</sup> self-assembled gels,<sup>38-41</sup> block copolymers,<sup>42</sup> telechelic polymers,<sup>43,44</sup> and ionomers,<sup>45</sup> however application of damage is difficult to interpret and measurements are often only characteristic of the applied flow. In contrast to typical shear measurements, extensional rheology allows for a definitive rupture of the material prior to robust, nonlinear rheological characterization.

In this work we examine the self-healing recovery process of entangled poly(*n*-butyl acrylate) and unentangled poly(methoxyethyl acrylate) melts which associate via hydrogen bonding, favored for its strength and robustness.<sup>16,46,47</sup> Using extensional rheology measurements

in both creep and constant rate of extension, we evaluate the role of the applied kinematic flow field and flow timescales on the measurement of recovery. We confirm the role of  $\tau_W$  and  $\tau_H$  on the recovery of the network as a function of network architecture and number of associations considering the model of Stukalin et al.<sup>13</sup> We outline the fundamental parameters needed to quantify the rheological nature of self-healing supramolecular polymer networks.

## Experimental Section

**Materials** Four model networks were used in this work. Poly(*n*-butyl acrylate), PnBA, was hydrolyzed to achieve random co-polymers of PnBA and poly(acrylic acid), PAA, with varying concentrations of PAA hydrogen bonding groups along the backbone. The details of this synthesis and rheological characterizations are available in previous works.<sup>29,33</sup> The current work utilizes the reference (or ‘pure’) PnBA (containing 3% PAA naturally<sup>29</sup>), and the synthesized nBA-AA (6%) and nBA-AA (38%) copolymers. These identical networks (except for number of associating groups) represent model entangled networks. The fourth network is a random copolymer of poly(methoxyethyl acrylate), PMEA, containing 3% 6-methyl-2-ureido-4[1H]-pyrimidone-bearing methacrylate groups, or UPyMA, obtained via free radical polymerization. The synthesis procedure and linear viscoelastic characterization for this system can be found in previous work.<sup>30</sup>

Table 1: Molecular weights, sticker compositions, and characteristic relaxation times of the polymer networks.

Polymer	$M_w$ (kDa)	PDI	$n_s$ (stickers/chain)	$M_s$ (kDa)	$\lambda$ (s)
MEA-UPyMA (3%)	32.1	2.9	2	16.0	$3 \times 10^{-6}$
PnBA	166	1.375	49	3.4	1.06
nBA-AA (6%)	161	1.375	90	1.8	1.16
nBA-AA (38%)	134	1.375	615	0.2	3.37

Table 1 highlights the important characteristics of the melts used in this work as reported in previously, where  $M_w$  is the molecular weight and  $PDI$  is polydispersity index. The

average number of hydrogen bonding groups, or stickers, per chain is represented by  $n_s$  and is determined by NMR spectroscopy.  $M_s$  represents the molecular weight of the sticky segment, i.e. the equivalent length of a chain attached to one associating group, calculated as  $M_w/n_s$ . The characteristic longest relaxation time of the melt is represented by  $\lambda$ . For nBA melts  $\lambda$  is the disengagement time,  $\tau_d$ , determined by fitting the BSW model to SAOS data.<sup>29</sup> For MEA-UPyMA (3%),  $\lambda = \tau_R$ , or the Rouse time, which is characteristic of the network backbone’s longest relaxation.<sup>30</sup>

**Extensional Rheology** Extensional rheology measurements were conducted using the VADER 1000 (*Rheo Filament ApS*). Cylindrical stainless steel sample plates with a diameter of 6 mm were used. The mass of each sample was on the order of 40 mg. Figure 1 illustrates the sample forming and testing procedure. Samples were first adhered to the top and bottom plates by heating the sample to 100°C under nitrogen purge and applying a moderate force. Samples were then pre-stretched from an initial aspect ratio of  $\Lambda_0 = L_0/R_0 = 0.167$  to approximately  $\Lambda = 1.33$ , after which the sample was slowly cooled to room temperature (22.5°C) and allowed to relax to zero stress. Filaments are then damaged by swiftly cutting the sample using a clean blade at the midpoint leaving two separate halves. The halves are maintained apart for some time, representing  $\tau_W$ . The halves are then contacted at fixed approach velocity  $u_c = 0.5\text{mm/s}$  until the desired contact force,  $F_c$ , is achieved. The optimum  $F_c$  has been chosen by examining the stress at break for two  $\tau_H$  for the most viscous network, MEA-UPyMA (3%), as shown in Figure S1 of the Supporting Information. As Figure S2 illustrates, there is a critical  $F_c$  required to achieve consistent measurements of the stress at break irrespective of  $\tau_H$ . We have selected  $F_c = 10\text{g}$  such that consistency is achieved but excess deformation is not applied during recovery. Constant position of the sample is held for the prescribed  $\tau_H$  after which the rheological characterization began.

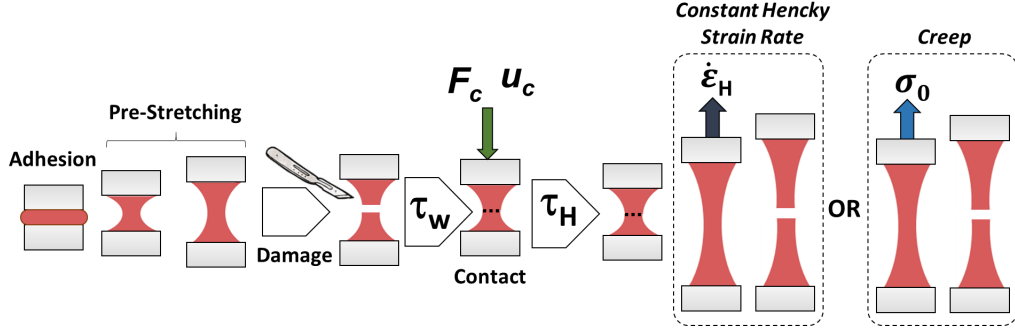


Figure 1: Schematic of the sample forming, healing, and testing protocols used in this work.

Two distinct rheological measurements were performed to probe recovery phenomena. Constant Hencky strain rate ( $\dot{\epsilon}_H$ ) experiments were conducted by continuous monitoring and control at the filament midplane.<sup>48</sup> Strain rates were varied between  $0.1\text{s}^{-1}$  and  $2.5\text{s}^{-1}$ . Creep experiments were conducted by maintaining constant stress,  $\langle\sigma_{zz} - \sigma_{rr}\rangle = \sigma_0$ , measured at the filament midplane. Creep stress was kept constant for all experiments at  $\sigma_0 = 5 \times 10^4\text{Pa}$ . In constant rate of extension, stress growth coefficients,  $\bar{\eta}^+(t)$  are calculated from measured stress and Hencky strain rate where  $\bar{\eta}^+(t) = \langle\sigma_{zz} - \sigma_{rr}\rangle(t)/\dot{\epsilon}_H$ . In creep, the compliance,  $\bar{J}$ , is calculated from measured strain and the applied stress such that  $\bar{J}(t) = \epsilon_H(t)/\sigma_0$ .  $\bar{\eta}^+(t)$  from creep experiments are calculated by smoothing  $\bar{J}(t)$  and performing the derivative where  $\bar{\eta}^+(t) = \left(\frac{\partial\bar{J}(t)}{\partial t}\right)^{-1}$ . Linear viscoelastic envelopes (LVE) are calculated using a multi-modal Maxwell model fit to SAOS data.<sup>29,30</sup> The LVE for  $\bar{\eta}^+(t)$  in constant rate of extension and creep are calculated separately according to (S7) and (S9), respectively, with more details given in the Supporting Information. Creep compliance LVEs are calculated according to (S8).<sup>49</sup> Time temperature superposition shift factors<sup>30,33</sup> were used to shift all LVEs and relevant timescales to the testing temperature of  $22.5^\circ\text{C}$  as necessary. All results are compared to the pristine material, defined as a sample which has been formed as described above but was kept intact before testing, representing the equilibrium state of the material.

Properties at break are determined at the point where the filament begins to rupture and are denoted as  $\bar{\eta}_{break}^+$ ,  $\sigma_{break}$ , and  $\epsilon_{H,break}$  for stress growth coefficient, the measured stress, and the strain at break, respectively. Additionally, we employ in our analysis both a stress ( $R_\sigma$ )

and a strain ( $R_\varepsilon$ ) recovery fraction defined as  $\sigma_{break}$  and  $\varepsilon_{H,break}$ , respectively, normalized by that of the pristine material under the same flow conditions. It should be noted that the  $R_\sigma$  is equivalently calculated using  $\bar{\eta}_{break}^+$  for constant rate of extension experiments. In order to consistently compare results, creep experiments are also summarized using  $R_\sigma$  calculated with  $\bar{\eta}_{break}^+$ , however, it is not equivalent to  $R_\sigma$  in terms of stresses in this case. This definition is necessary to account for the varying strain rates achieved as a function of time for different materials and degrees of recovery measured at the same stress. Examples of these transient strain rates are shown in Figure S5 for all melts.

## Results

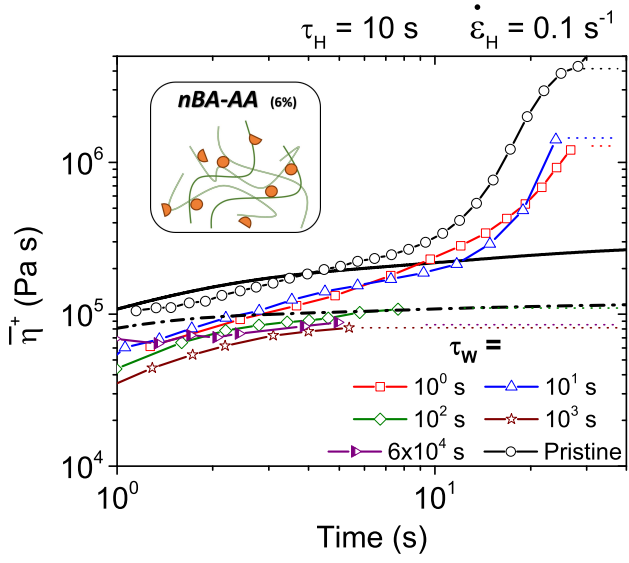
### The Effect of $\tau_W$ on Recovery

When a reversibly crosslinked network is damaged and contact is not immediately reestablished, both association and chain dynamics alter the state of the freshly damaged surfaces. We expect stress recovery to strongly depend on  $\tau_W$ . According to Rubinstein’s model,<sup>13</sup> the recovery of the network should decrease with increasing  $\tau_W$  for fixed  $\tau_H$ . This is because at long  $\tau_W$ , dangling chains have sufficient time to internalize stickers.

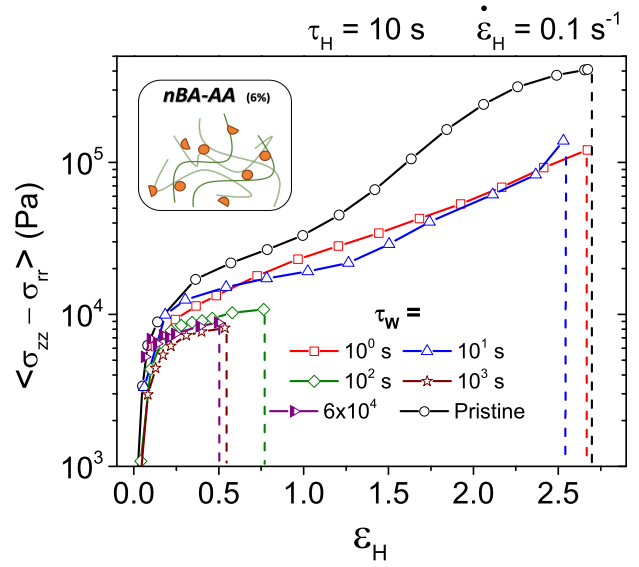
*Entangled Network:* Figure 2a shows the effect of  $\tau_W$  on  $\bar{\eta}^+(t)$  of nBA-AA (6%) for a fixed  $\tau_H = 10$ s, which is approximately  $10\lambda$ , suggesting full relaxation of entanglements. For  $\tau_W < 10^2$ s, the network shows similar strain hardening behavior to the pristine network. For  $\tau_W \geq 10^2$ s,  $\bar{\eta}^+(t)$  is significantly smaller than the pristine material response. More importantly,  $\bar{\eta}^+(t)$  is below the LVE for nBA-AA (6%). In fact,  $\bar{\eta}^+(t)$  appears to have no contributions from associating groups, i.e. follows the same response as pure PnBA (dash-dot line). The same trends can be observed in Figure 2b in terms of measured stress versus applied strain. This figure highlights the dependence of  $\varepsilon_{H,break}$  on  $\tau_W$ . For increasing values of  $\tau_W$  the network becomes significantly more brittle and breaks at low Hencky strain.

*Unentangled Network:* Figure 2c and 2d show the same experimental procedure as applied

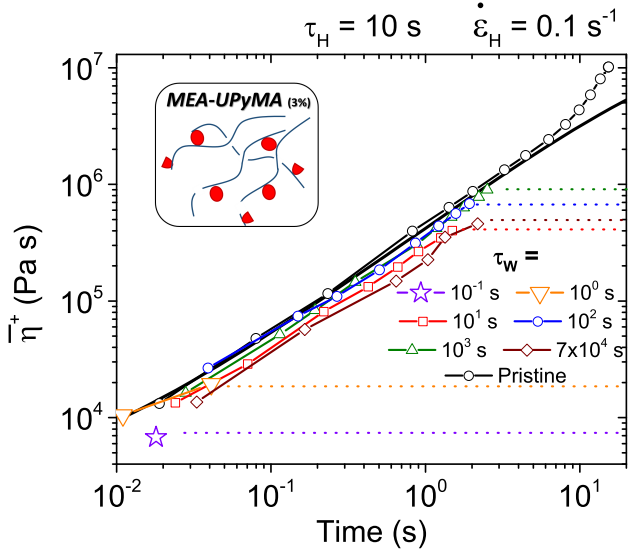
to MEA-UPyMA (3%). Unlike for nBA-AA (6%),  $\bar{\eta}^+(t)$  follows the LVE for all values of  $\tau_W$ . The pristine MEA-UPyMA shows very little strain hardening compared to nBA-AA and the network fractures at small strains for  $\dot{\varepsilon}_H = 0.1\text{s}^{-1}$ . Strain hardening in linear polymer chains is not typically seen below  $\varepsilon = 1$ <sup>50</sup> and therefore insignificant recovery is expected to give a response which follows the LVE before breaking. While stress increases similarly for all  $\tau_W \leq 10^3\text{s}$ ,  $\tau_W = 7 \times 10^4\text{s}$  shows different dynamics. Another important difference between MEA-UPyMA and nBA-AA is that we observe an increasing  $\bar{\eta}_{break}^+$  with increasing  $\tau_W$  for  $\tau_W \leq 10^3\text{s}$  for MEA-UPyMA. For  $\tau_W = 7 \times 10^3\text{s}$ , we see that  $\bar{\eta}_{break}^+$  starts to decrease again as observed in the case of nBA-AA (6%).



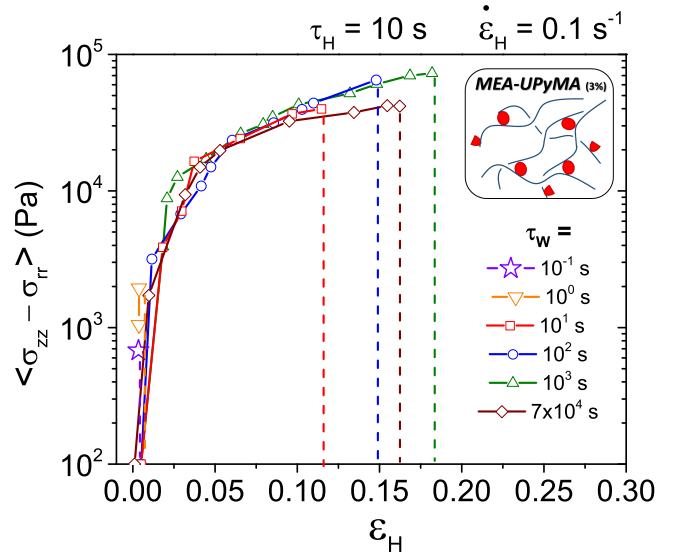
(a)



(b)



(c)



(d)

Figure 2: The effect of  $\tau_W$  on  $\bar{\eta}^+(t)$  (a,c) and stress-strain behavior (b,d) of nBA-AA (6%) and MEA-UPyMA (3%). The solid lines represent the LVE of the pristine network. The dash-dot line represents the LVE of pure PnBA. Broken lines represent approximate  $\bar{\eta}_{break}^+$  and  $\epsilon_{H,break}$ .

## The Effect of $\tau_H$ on Recovery of Entangled Networks

For all subsequent healing measurements, we fix  $\tau_W$ . For nBA-AA (6%),  $\tau_W \geq 10^3$  s is used because recovery is no longer dependent on  $\tau_W$ . Here  $\tau_W \approx \tau_{eq}$  which, according to Stukalin

et al., is expected to show a monotonically increasing number of bridges across the interface with increasing  $\tau_H$ .<sup>13</sup> For MEA-UPyMA (3%)  $\tau_W \approx 10^3$ s is used, at which time the maximum recovery with respect to  $\tau_W$  is achieved. This gives  $\tau_W \approx \tau_b$  which is expected to give more complex bridge formation dynamics as a function of  $\tau_H$ . From theory we expect the recovery of the mechanical properties of the network to be related to the number of interfacial bridges which have reformed. We use nonlinear extensional flow to probe the material properties using either constant stress or constant rate experiments. Typically tensile measurements are performed at constant velocity, which do not control the kinematics of the flow field. Using the VADER 1000, we control the kinematic flow and therefore are interested in comparing the recovery of the material in both flow fields.

**Creep.** We first probe the effect of number of hydrogen bonding groups per chain on recovery dynamics using creep compliance, i.e.  $\bar{J}(t)$ , and calculate stress growth coefficients  $\bar{\eta}^+(t)$  as discussed in the Experimental Section. Figure 3a and 3b show the response for pure PnBA. All compliance curves resemble a response typical of an amorphous polymer of low molecular weight. Furthermore, the shift of the compliance curve to higher times with  $\tau_H$  is similar to a shift due to increasing molecular weight: suggesting increasing number of entanglements.<sup>51</sup> Figure 3a shows that for  $\tau_H \leq 4 \times 10^0$ s the compliance curve is steeper than the pristine material response. For  $\tau_H > 4 \times 10^0$ s the compliance curves follow the pristine material near the point of fracture. Non-linear behavior is seen at long times for  $\tau_H > 4 \times 10^0$ s. Figure 3b shows the corresponding  $\bar{\eta}^+(t)$  where the transition with  $\tau_H$  is more noticeable.  $\tau_H < 4 \times 10^0$ s shows a similar trend to the LVE of pure PnBA, while  $\tau_H > 2 \times 10^1$ s shows very similar strain hardening behavior to the pristine material. Note that in creep, we expect that  $\bar{\eta}^+(t)$  approaches  $3\eta_0$  faster than in constant rate of extension.<sup>49,52</sup> However, at short experimental times creep  $\bar{\eta}^+(t)$  does not follow the creep LVE because start-up of the constant stress flow leads to non-creep behavior, as highlighted in Figure S4a and S4b and explained further in Supporting Information.

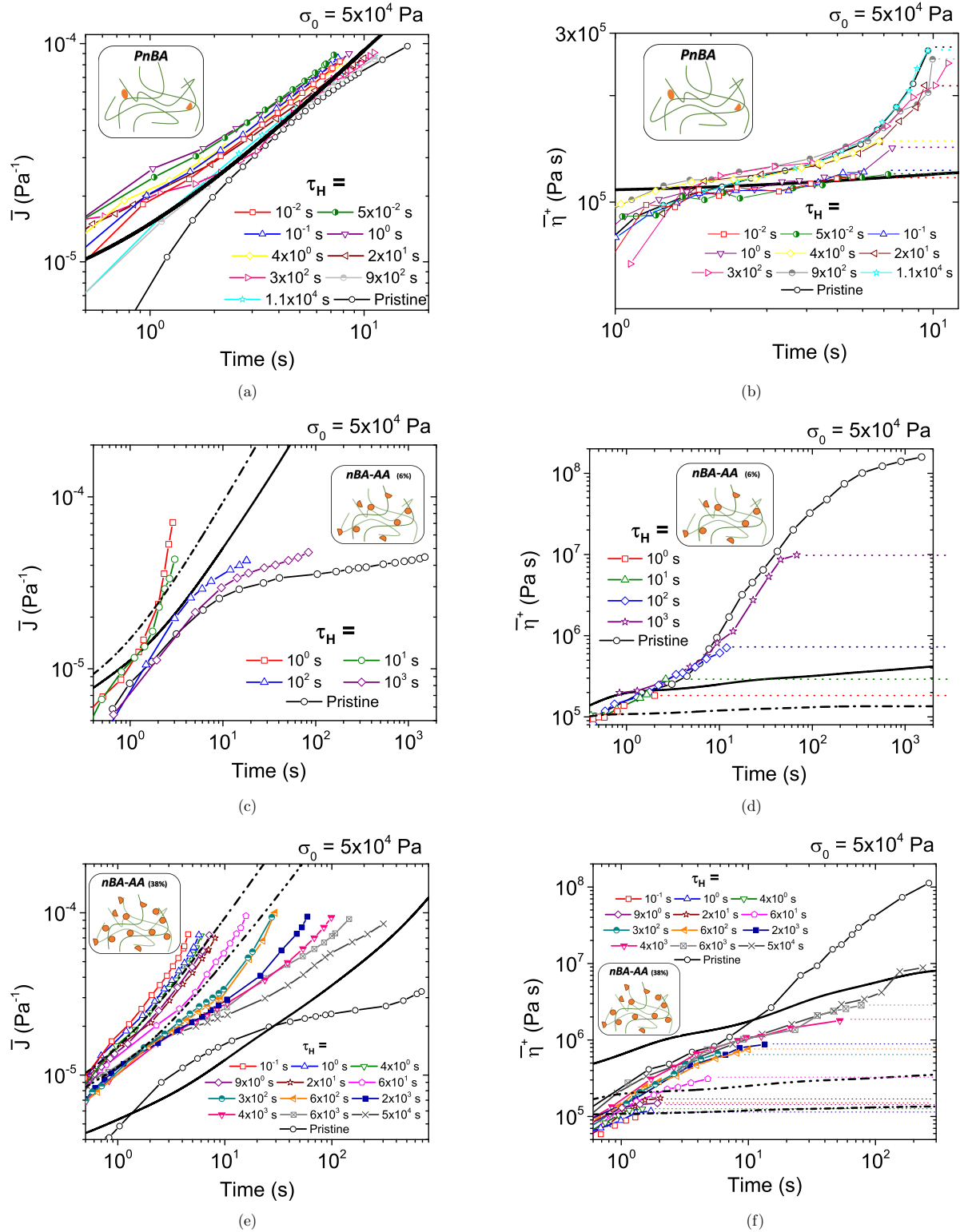


Figure 3: The effect of  $\tau_H$  on creep response of entangled PnBA networks in  $\bar{J}(t)$  and  $\bar{\eta}^+(t)$ . The solid lines represent the LVE of the pristine material for each plot. The dash-dot lines in (c)-(f) represent the nBA-AA (6%) LVE. The dash-dot-dot lines in (e)-(f) represent the nBA-AA (38%) LVE. Broken lines represent approximate  $\bar{\eta}^+$  at break.

nBA-AA (6%) contains a moderate number of hydrogen bonding groups with an identical backbone to pure PnBA. The compliance curves for this material are shown in Figure 3c. At low healing time,  $\tau_H = 10^0$ s, the material is more compliant than pure PnBA, suggesting that frictional effects dominate and few associations are recovered. At  $\tau_H = 10^1$ s, the material has a compliance that is very similar to pure PnBA for the same applied stress (see Figure 3a), but breaks at earlier time (lower strain). Increasing  $\tau_H$  shows a drastic turnover in compliance; suggesting the recovery of associations across the fractured interface. Qualitatively above  $\tau_H > 10^1$ s, the compliance resembles a moderately crosslinked network, whereby crosslink density increases with  $\tau_H$ .<sup>51</sup> The similarity of compliance of nBA-AA (6%) to pure PnBA at low  $\tau_H$  is very clearly shown in Figure 3d in terms of  $\bar{\eta}^+(t)$ . For  $\tau_H = 10^0$ s, strain hardening with respect to the pure PnBA LVE (dash-dot line) is achieved. For  $\tau_H = 10^1$ s only slight strain hardening occurs with respect to pristine nBA-AA (6%) LVE, whereas  $\tau_H \geq 10^1$ s shows higher degrees of strain hardening. It is known that increased viscosity of this network is largely a function of degree of association,<sup>29</sup> thus reduced compliance and increasing  $\bar{\eta}_{break}^+$  is directly proportional to recovery of hydrogen bonds with  $\tau_H$ .

Compliance curves for nBA-AA (38%) are shown in Figure 3e. As with the previous two networks, the compliance for short  $\tau_H$ , i.e.  $\tau_H \leq 9 \times 10^0$ s, resembles that of pure PnBA for  $\sigma_0 = 5 \times 10^4$ Pa. At  $\tau_H = 9 \times 10^0$ s the compliance is almost identical to the LVE of pure PnBA (see dash-dot line). For  $2 \times 10^1 \geq \tau_H \leq 6 \times 10^1$ s,  $\bar{J}(t)$  further decreases with  $\tau_H$ , approaching the nBA-AA (6%) LVE at long times (dash-dot-dot line). For  $\tau_H > 6 \times 10^1$ s, an order of magnitude increase in  $\tau_H$  only slightly decreases  $\bar{J}(t)$  as we slowly approach full recovery (see pristine response). The stress growth coefficients,  $\bar{\eta}^+(t)$ , for the data set are shown in Figure 3f. It is clear that for short  $\tau_H$  ( $\leq 2 \times 10^1$ s) the material is breaking at  $\bar{\eta}_{break}^+$  approximately equal to  $3\eta_0$  of pure PnBA. For  $\tau_H \geq 6 \times 10^1$ s strain hardening is observed. The degree of strain hardening limited by  $\bar{\eta}_{break}^+$  is increasing steadily with  $\tau_H$ . Only for  $\tau_H = 5 \times 10^4$ s does  $\bar{\eta}^+(t)$  approach the LVE of pristine nBA-AA (38%) at long times, suggesting that full recovery requires much longer times.

**Constant Rate of Extension.** Constant rate of extension ( $\dot{\epsilon}_H$ ) was used to measure recovery of nBA-AA (6%). Figure 4a shows  $\bar{\eta}^+(t)$  for varied  $\tau_H$  and constant  $\dot{\epsilon}_H = 0.1\text{s}^{-1}$ . At all  $\tau_H$ ,  $\bar{\eta}^+(t)$  follows a master curve (equivalent to the pristine response) up to the material breaking point. For  $\tau_H \leq 10^0\text{s}$ ,  $\bar{\eta}_{break}^+$  is low and breaking occurs along the LVE. For  $\tau_H > 10^0\text{s}$ , much higher  $\bar{\eta}_{break}^+$  are obtained with behavior that is approximately the same as that of the pristine material. There is little difference between the  $\bar{\eta}_{break}^+$  for measurements where  $\tau_H \geq 10^2\text{s}$ . The stress-strain behavior in Figure 4b shows low  $\epsilon_{H,break}$  for  $\tau_H \leq 10^0\text{s}$ . For  $\tau_H \geq 10^2\text{s}$ , high  $\epsilon_{H,break}$  are achieved and are nearly identical to each other and to the pristine material. This behavior is fundamentally different from that seen for creep measurements. Whereas in creep both  $\bar{\eta}^+(t)$  and  $\bar{J}(t)$  vary as a function of  $\tau_H$ , in constant rate of extension,  $\bar{\eta}^+(t)$  is a master curve with varying  $\bar{\eta}_{break}^+$  and  $\epsilon_{H,break}$ . Additionally, recovery of the pristine material response is achieved at much shorter healing times, ( $\tau_H \approx 10^2\text{s}$ ), whereas in creep very little recovery of the material is observed for two orders of magnitude higher healing times.

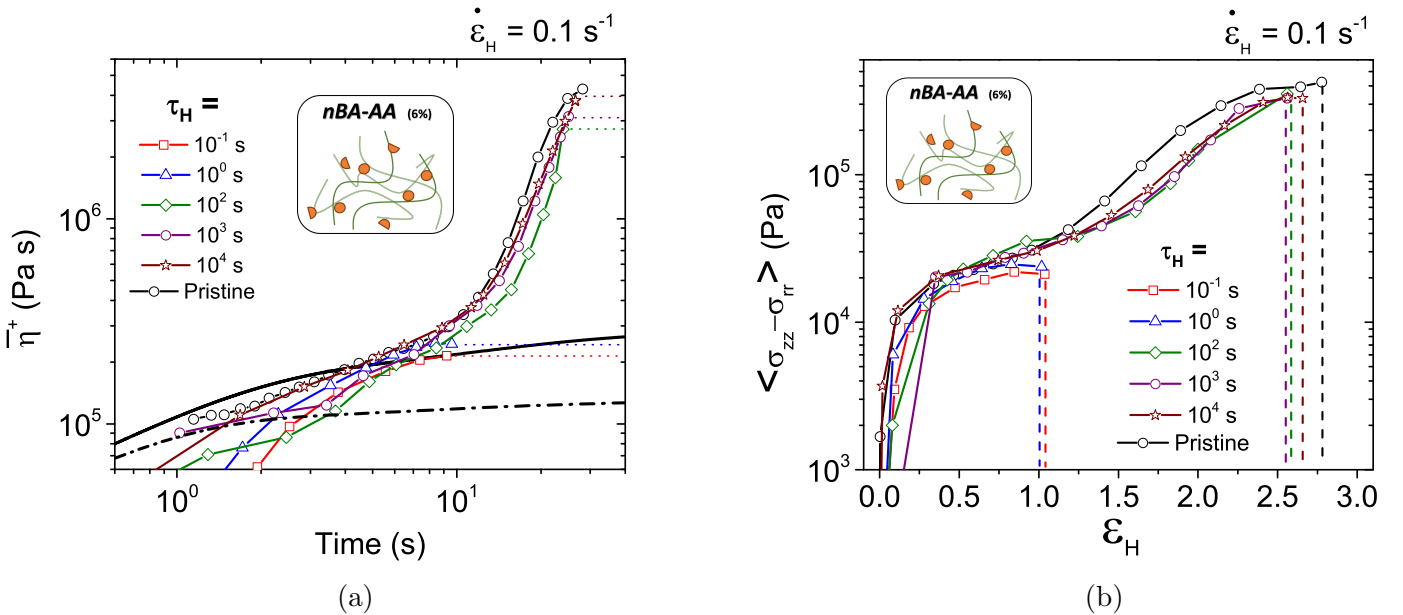
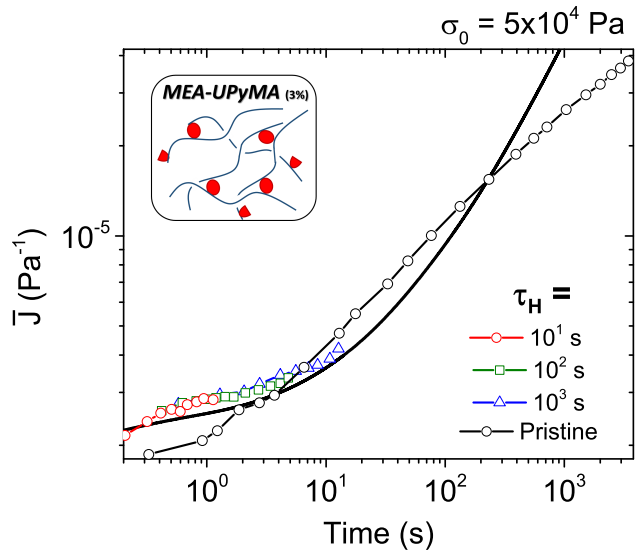


Figure 4: The effect of  $\tau_H$  on nBA-AA (6%) under constant rate of extension,  $\dot{\epsilon}_H = 0.1\text{s}^{-1}$ . The solid line represents the LVE for nBA-AA (6%) and the dash-dot line for pure PnBA. Broken lines represent approximate  $\bar{\eta}_{break}^+$  and  $\epsilon_{H,break}$ .

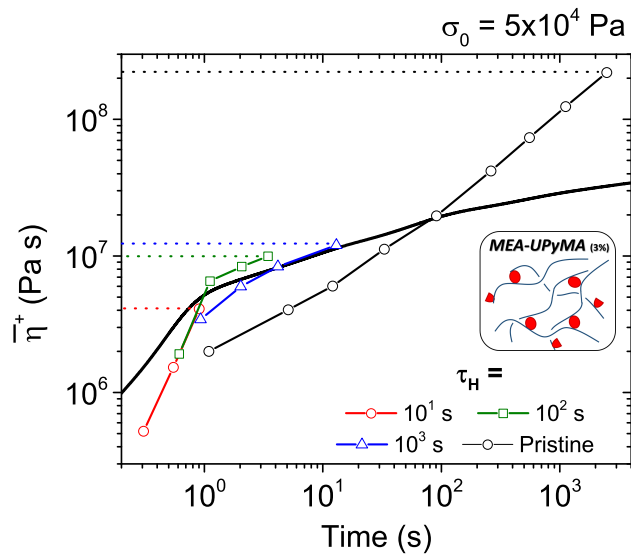
## The Effect of $\tau_H$ on Recovery of Unentangled Networks

We now explore a network composed of PMEA backbones, which compared to the PnBA based polymers is essentially free of entanglements. For example, the linear viscoelastic response of pure PMEA follows that of an unentangled melt.<sup>30</sup> Figure 5a shows creep compliance for MEA-UPyMA (3%). For all  $\tau_H$ ,  $\bar{J}(t)$  approximately follows the LVE. With increasing  $\tau_H$ , increasing compliance is achieved, however  $\bar{J}(t)$  remains about an order of magnitude lower than the pristine material. The very low compliance is most likely due to the absence of reformed associations and the lack of entanglements to sustain the stress. Only when associations have sufficiently recovered (long  $\tau_H$ ) can the network distribute load continuously across the interface, leading to higher extensibility.  $\bar{\eta}^+(t)$  shown in Figure 5b all follow the LVE up to  $\bar{\eta}_{break}^+$  which increases with  $\tau_H$ . At no  $\tau_H$  does strain hardening occur and  $\bar{\eta}_{break}^+$  is more than an order of magnitude lower than that of the pristine material.

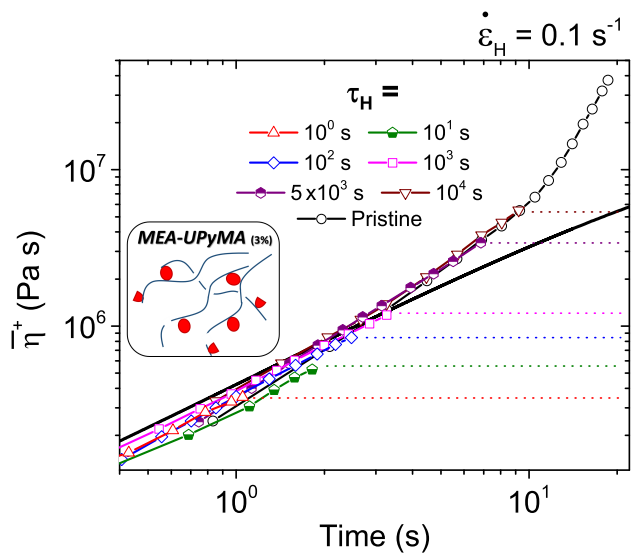
Figure 5c shows the effect of  $\tau_H$  on MEA-UPyMA (3%) measured at constant rate of extension.  $\bar{\eta}^+(t)$  follows the pristine material response for all  $\tau_H$ . With increasing  $\tau_H$ , higher  $\bar{\eta}_{break}^+$  are achieved, however significant strain hardening is only achieved for  $\tau_H > 10^3$ s. Stress-strain curves (Figure 5d) highlight increasing  $\varepsilon_{H,break}$  with increasing  $\tau_H$ . As with creep for  $\tau_H < 10^3$ , healed responses are identical to the LVE up to  $\bar{\eta}_{break}^+$ . However, unlike for PnBA networks, the unentangled network exhibits the same qualitative behavior for both creep and extension, but the degree of recovery is different.



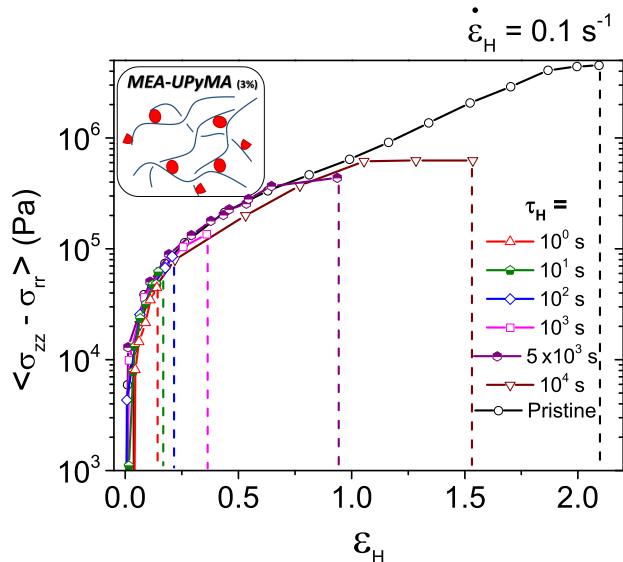
(a)



(b)



(c)



(d)

Figure 5: The effect of  $\tau_H$  on MEA-UPyMA (3%) in creep (a-b) and in constant rate of extension (c-d). Solid lines represent the MEA-UPyMA (3%) LVE. Broken lines represent approximate  $\bar{\eta}_{break}^+$  and  $\varepsilon_{H,break}$ .

# Discussion

## The Effect of $\tau_W$ on Recovery

According to Stukalin et al., the recovery of associations depends strongly on the relative magnitude of  $\tau_W$  compared to timescales of the polymer. The three important timescales of the polymer are the Rouse time  $\tau_R$ , bond lifetime  $\tau_b$ , and the equilibration time  $\tau_{eq}$ . Critical timescales are calculated as described in Stukalin et al.<sup>13</sup> (see (S2)-(S5) in Supporting Information) and are reported in Table 2.

Figure 6 summarizes relative recovery in terms of stress and strain of MEA-UPyMA (3%) and nBA-AA (6%) as a function of  $\tau_W/\tau_b$ . The normalized values of  $\tau_R$  and  $\tau_{eq}$  are indicated via arrows in Figure 6. According to Stukalin et al., we expect a plateau in recovery for  $\tau_W/\tau_b < 1$  and a sudden decrease in recovery for  $\tau_W/\tau_b > 1$ . Ultimately for  $\tau_W/\tau_b > \tau_{eq}/\tau_b$  there is again no change in the amount of recovery for a constant  $\tau_H$ . The physical argument is that for  $\tau_W/\tau_b > 1$  the free associations begin to find internal partners, which means less associations are available to form bridges at the interface. For  $\tau_W > \tau_{eq}$ , an equilibrium number of free associations have found internal partners leaving an equilibrium number of free associations available at the interface for all increasing  $\tau_W$ . Examining the recovery of nBA-AA (6%) shows for  $\tau_R/\tau_b < \tau_W/\tau_b < 1$  recovery is constant with increasing  $\tau_W$ . For  $1 < \tau_W/\tau_b < \tau_{eq}/\tau_b$  there is an overall decrease in recovery of stress and strain. For  $\tau_W/\tau_b > \tau_{eq}/\tau_b$ , no change in recovery is seen with increasing  $\tau_W$ . The data suggest that the results for nBA-AA (6%) are in excellent agreement with the arguments made by Rubinstein and coworkers. Note that many other works have observed a decrease in recovery with  $\tau_W$ , but no systematic study has shown the plateau regions.<sup>14,16,53-58</sup>

Table 2: Calculated timescales of the associating polymer networks.

	nBA-AA (6%)	MEA-UPyMA (3%)
$\tau_0$	$4 \times 10^{-4}$	$2 \times 10^{-10}$
$\tau_R$	$4 \times 10^{-2}$	$3 \times 10^{-6}$
$\tau_b$	$6 \times 10^1$	$4 \times 10^2$
$\tau_{eq}$	$2 \times 10^3$	$4 \times 10^6$
$\tau_{adh}$	$7 \times 10^3$	$4 \times 10^7$

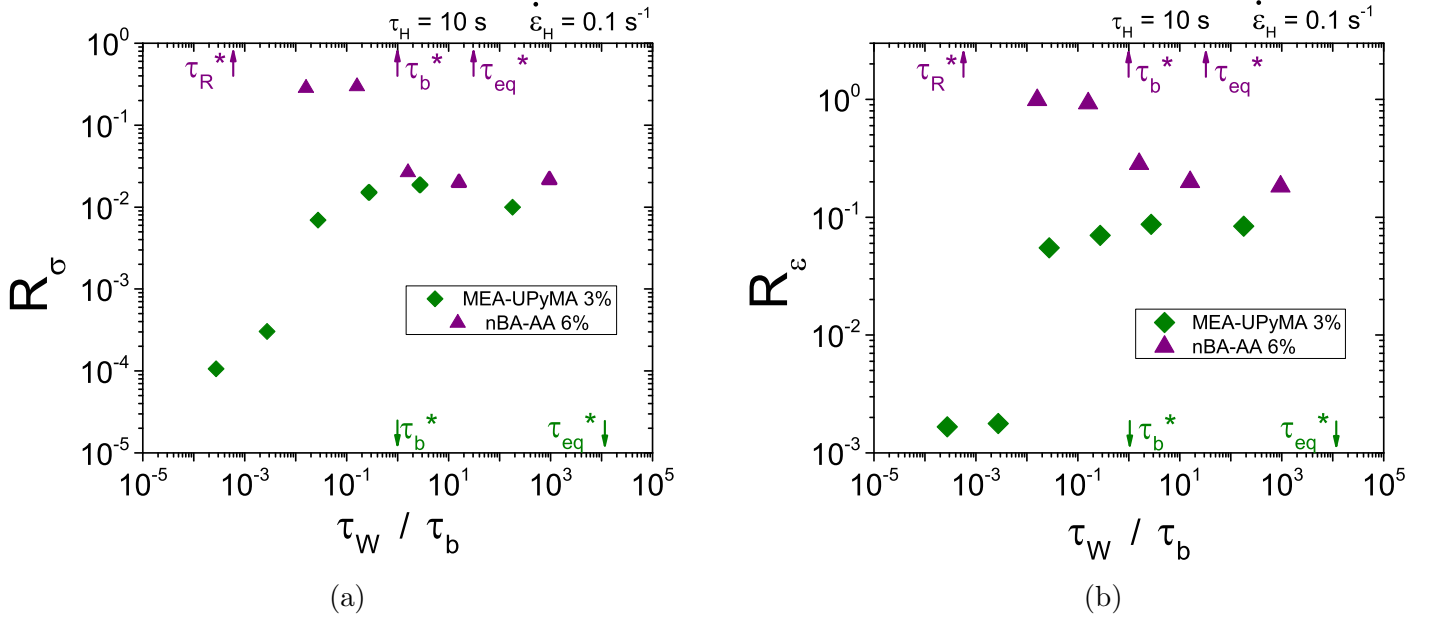


Figure 6: Stress and strain recovery of MEA-UPyMA (3%) and nBA-AA (6%) as a function of  $\tau_W/\tau_b$  for  $\tau_H = 10$ s under constant rate of extension  $\dot{\epsilon}_H = 0.1$ s. Arrows indicate normalized polymer timescales (see Table 2) for MEA-UPyMA (3%) on the lower axes and nBA-AA (6%) on the upper axes.

Interestingly MEA-UPyMA (3%) data show an unexpected increase in stress and strain recovery for  $\tau_W/\tau_b < 1$  followed by an expected decrease in recovery for  $\tau_W/\tau_b > 1$ . We hypothesize that this contradictory trend is possibly due to irreversible damage to the chemical bonds within the backbone during break. In both cases, the damaged samples were created by cutting the material with a razor blade. As a result, the damage surface is likely comprised of broken chains.<sup>59</sup> While open stickers are present at the interface, their effect on recovery is limited because of their low concentration in the case of MEA-UPyMA. Thus we observe an increase in the recovery due to diffusion of nearby free associations to the interface

on the timescale of  $\lambda/\tau_b \approx 3 \times 10^{-1}$ . We suspect that this is not observed in nBA-AA due to the much higher concentration of associating groups per chain and the faster diffusion of free associations,  $\lambda/\tau_b \approx 2 \times 10^{-2}$ .

## The Effect of $\tau_H$ on Recovery

The effect of  $\tau_H$  on recovery of PnBA networks in creep can be evaluated by comparing  $\bar{\eta}_{break}^+$ , as shown in Figure 7. While convention dictates a stress at break is more appropriate, constant stress measurements vary only in strain and strain rate, leaving stress growth coefficient for comparison.  $\tau_H$  is scaled by  $\lambda$ , the characteristic longest relaxation time for the polymer melts, to highlight the role of entanglements. Recall that  $\lambda$  was shown to dictate the role of associations on extensional flow by Shabbir et al.<sup>29</sup> For  $\tau_H/\lambda < 10$ , all melts form a master curve of  $\bar{\eta}_{break}^+$  suggesting that all three melts are undergoing the same healing dynamics (i.e. reformation of entanglements across the interface). For  $\tau_H/\lambda > 10$ , a plateau for pure PnBA at the pristine material  $\bar{\eta}_{break}^+$  is observed, which is indicative of full recovery of entanglements. For  $\tau_H/\lambda > 10$ , both nBA-AA 6% and 38% show  $\bar{\eta}_{break}^+$  increasing substantially over pure PnBA, approaching their own pristine values (dotted lines) with increasing  $\tau_H$ . These measurements show clearly that recovery is sequential, beginning with re-entanglement dynamics across the interface, followed by re-association of hydrogen bonding groups. Note that for the longest  $\tau_H$ , measurements are in the regime of  $\tau_H > \tau_{adh}$ , however recovery is not complete as predicted by the work of Stukalin et al.<sup>13</sup> This is likely due to the presence of entanglements which must repeatedly relax in order to free up associations at the interface, which is not accounted for in the original model.

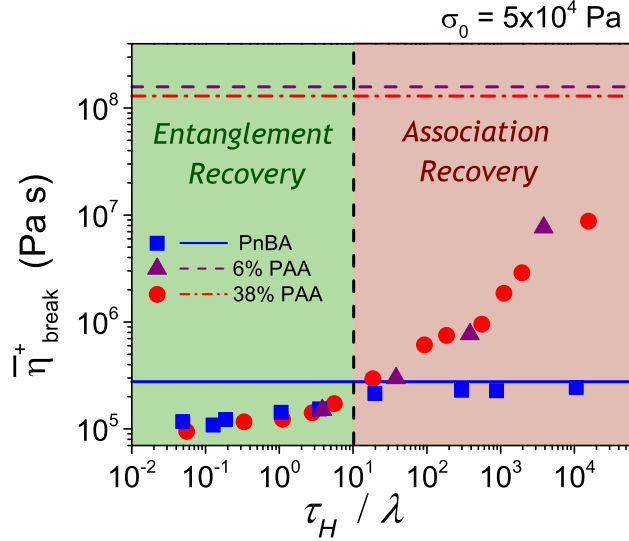


Figure 7:  $\bar{\eta}_{break}^+$  for all PnBA networks measured in creep. Lines represent pristine material  $\bar{\eta}_{break}^+$  for each network.

## The Effect of Applied Kinematics on Recovery

We now evaluate the role of kinematics on the measurement of recovery by comparing the results of constant rate of extension with that of creep for nBA-AA 6% and MEA-UPyMA 3%. Figure 8 summarizes the stress and strain recovery of nBA-AA (6%) as a function of  $\tau_H$ . Note that an additional dataset is included in Figure 8 at  $\dot{\epsilon}_H = 2.5\text{s}^{-1}$  which is not reported in the results section (but available in Figure S6). It is evident that for the selected range of  $\tau_H$ , measured stress recovery is much lower for creep ( $R_\sigma < 10\%$ ) than for constant  $\dot{\epsilon}_H$  ( $R_\sigma > 40\%$ ). At constant rate, a sudden increase in  $R_\sigma$  occurs at  $\tau_H \approx 10\lambda$ , followed by relatively constant  $R_\sigma$  for long  $\tau_H$ .

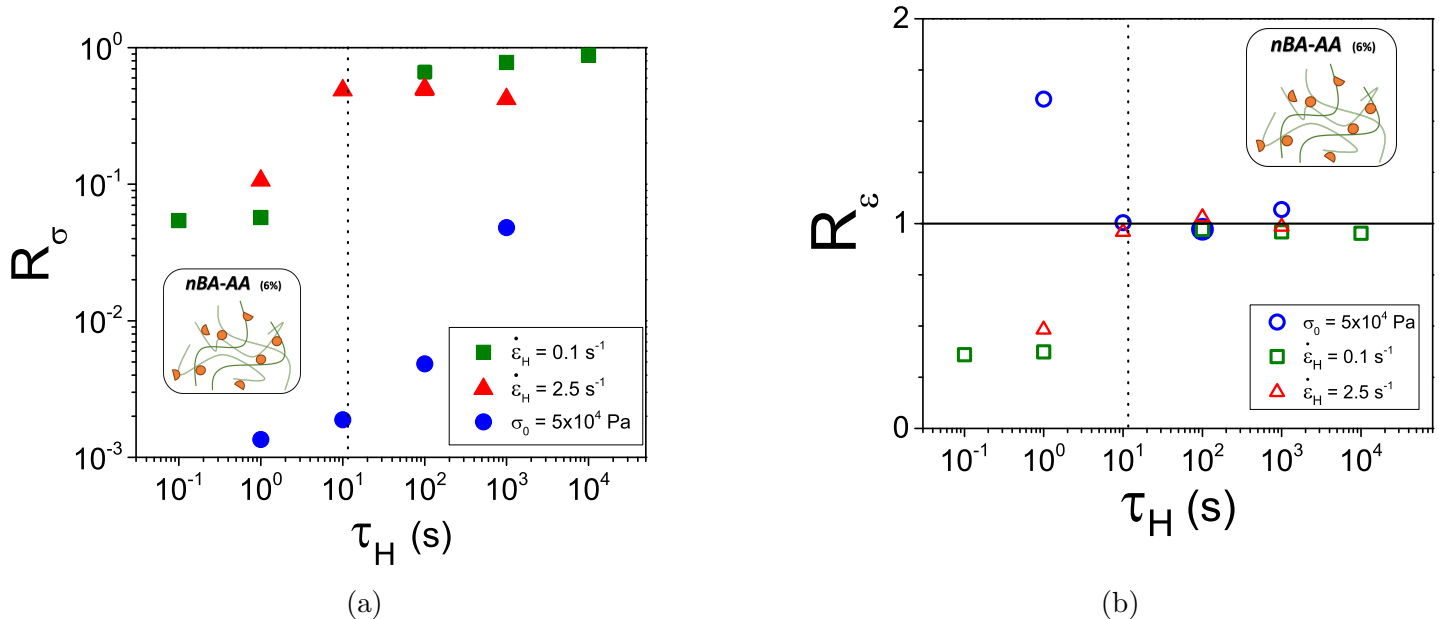


Figure 8: The effect of  $\tau_H$  on stress and strain recovery for nBA-AA (6%) in creep and constant rate of extension. Dotted lines indicate  $\tau_H \approx 10\lambda$ .

We do not expect flow kinematics to impact degree of recovery when probed in the linear viscoelastic regime. However, the importance of association dynamics at very large timescales (low frequency) make it very difficult to probe the LVE (see Shabbir et al.<sup>29,30</sup>). Thus all strain-rates probe some non-linear response of the melts. Figure 8 clearly shows that the nonlinear response and thus nonlinear *measured* recovery strongly depends on the timescale of the flow. In creep, a single stress probes a spectrum of retardation times,<sup>51,52,60</sup> while constant rate of extension is said to probe only relaxations occurring at timescales slower than the flow timescale. In unassociating linear polymers, rates of extension faster than the inverse Rouse time induce chain stretch and entanglements dominate the measurement.<sup>34,61,62</sup> For nBA-AA, entanglements are argued to be fully recovered at about  $\tau_H \approx 10\text{s}$ . The sharp increase in  $R_\sigma$  observed at  $\tau_H \approx 10\text{s}$  suggests that the response is strongly dependent on the presence of entanglements and is relatively insensitive to recovery of associations, which gradually increase recovery. The measured recovery probed in creep is orders of magnitude smaller than in constant rate of extension. In creep, the response is characteristic of the entire material for a wide range of timescales (both long and short). While in constant rate

of extension we focus on entanglement dynamics, creep is probing the sequential buildup of entanglements and associations equally. This is most clearly seen in the build up of material compliance in Figure 3 where entanglement dynamics and association dynamics are distinguishable.

Strain recoveries,  $R_\epsilon$ , in Figure 8b further highlight this phenomenon. For constant  $\dot{\epsilon}_H$  and  $\tau_H < 10\text{s}$ ,  $R_\epsilon$  is substantially lower than full recovery ( $R_\epsilon < 1$ ). Further recovery shows an increase in  $R_\epsilon$  and then an immediate plateau of extensibility. In creep for  $\tau_H < 10\text{s}$ ,  $R_\epsilon$  starts off higher than full recovery. Further recovery shows a decrease in  $R_\epsilon$  until again a plateau in extensibility is reached. The plateau in  $R_\epsilon$  supports the argument that entanglements are solely responsible for the extensibility of the network. Associations do however affect the stress required to achieve a degree of extensibility. This is better seen in the absence of entanglements.

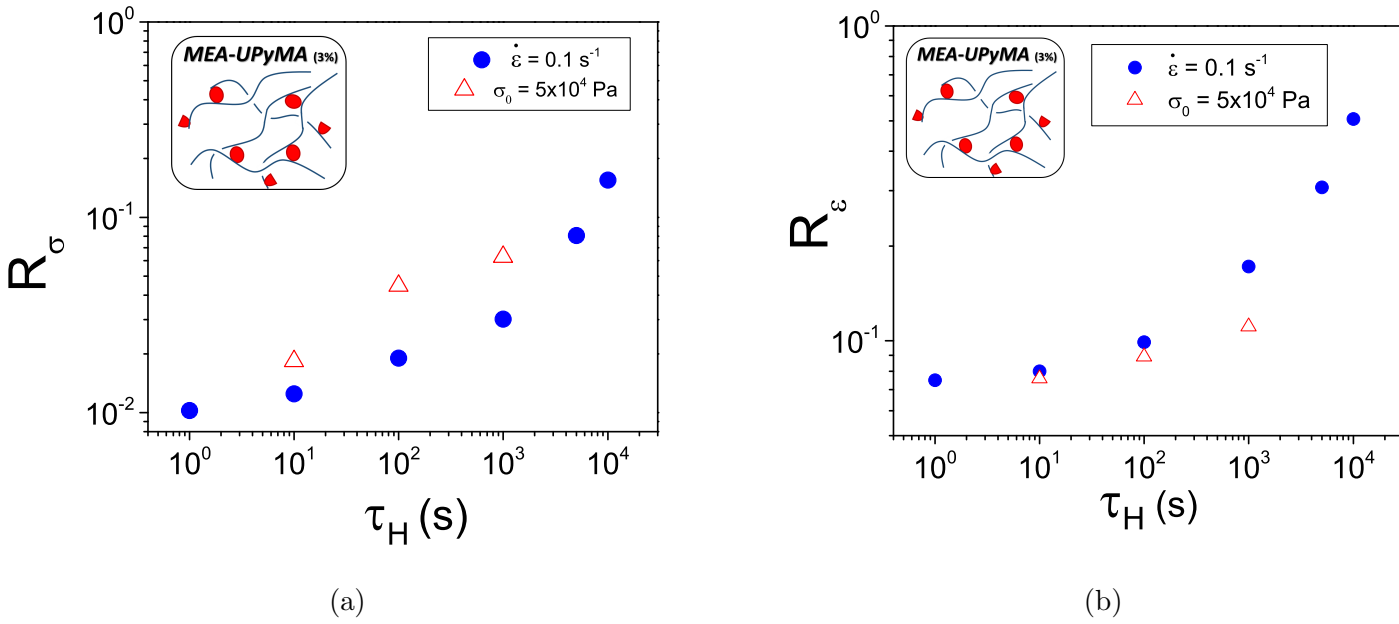


Figure 9: The effect of  $\tau_H$  on stress and strain recovery for MEA-UPyMA (3%) in creep and constant rate of extension.

Figure 9a summarizes the stress and strain recovery as a function of  $\tau_H$  for both creep and constant rate of extension for unentangled MEA-UPyMA (3%). Comparable trends in stress and strain recovery are observed for both creep and constant rate experiments. These results

show clear differences from nBA-AA (6%), namely  $R_e$  is much lower and is steadily increasing as a function of  $\tau_H$ . We argue that since hydrogen bonds rather than entanglements are responsible for stress buildup in MEA-UPyMA, all flows are probing the number of re-associated bonds. In other words, the measured recovery of MEA-UPyMA (3%) does not depend on the applied flow. Furthermore, the extensibility of an unentangled network is dependent on the number of associations, whereas an entangled network has a critical strain that is proportional to the number of entanglements. This clearly shows that stress and strain recovery do not always probe the same mechanisms or measure the true recovery of the material. Stress recovery is much more indicative of the material behavior than strain recovery. Furthermore, true and measured recovery are independent properties and measured recovery can depend strongly on the chemical structure, measurement technique, and kinematics of flow. Making correlations between measured recovery and true recovery is still a challenge and must be explored further.

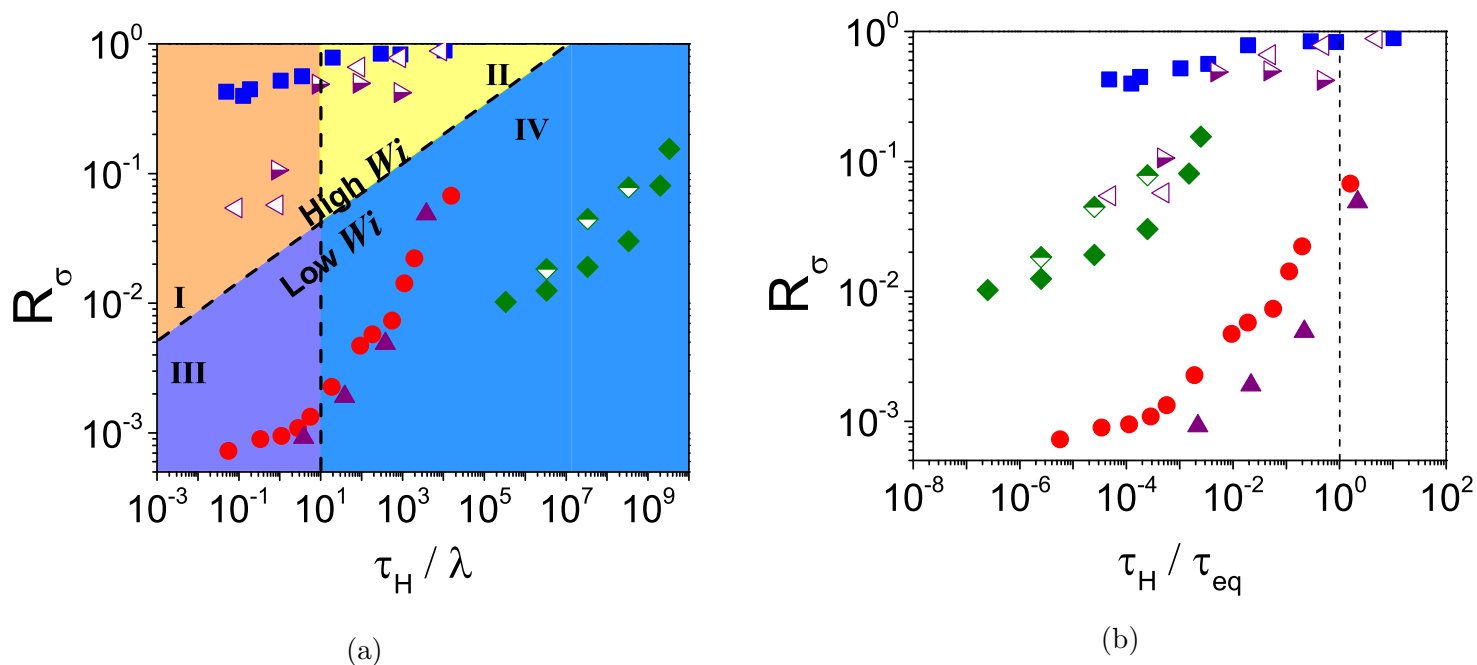


Figure 10: Summary of recovery for all networks with respect to (a) chain dynamics and (b) association dynamics. See legend in Table 3.

Table 3:  $Wi$  for all kinematics and networks in this work.

$\sigma_0 = 5 \times 10^4 \text{Pa}$		$Wi$	$\dot{\epsilon}_H = 0.1 \text{s}^{-1}$		$Wi$	$\dot{\epsilon}_H = 2.5 \text{s}^{-1}$		$Wi$
■	PnBA	$2 \times 10^{-1}$	◁	nBA-AA (6%)	$1 \times 10^{-1}$	▷	nBA-AA (6%)	$3 \times 10^0$
▲	nBA-AA (6%)	$3 \times 10^{-4}$	◆	MEA-UPyMA (3%)	$3 \times 10^{-7}$			
●	nBA-AA (38%)	$1 \times 10^{-3}$						
◆	MEA-UPyMA (3%)	$6 \times 10^{-10}$						

We now bring together all measured data of stress recovery for the different chemistries presented here. Figure 10a summarizes the stress recovery as a function of normalized healing time ( $\tau_H/\lambda$ ) for all networks and flows studied in this work. Here we employ a Weissenberg number,  $Wi = \lambda \dot{\epsilon}_H$ , to quantify the applied flow with respect to characteristic polymer relaxation. For creep, we use the asymptotic strain rate, defined as  $\dot{\epsilon}_H = \left(\frac{\partial \epsilon_H}{\partial t}\right)_{t \rightarrow \infty}$  to define the Weissenberg number. Note that in creep experiments, the strain-rate starts very high and decays in exponential manner with time (see Figure S5). We separate experiments into four regimes determined by applied flow (high vs. low  $Wi$ ) and three mechanisms of recovery: I and III represent dynamic relaxation of entanglements, II represents relaxed entanglements, and IV represents dynamic recovery of associations.

For  $\tau_H$  shorter than the characteristic relaxation time of the polymer, i.e  $\tau_H/\lambda < 10$ , (regimes I and III) the stress recovery is dominated by entanglement recovery with little to no recovery of associations. In regime II, the stress recovery of nBA-AA networks shows almost full recovery since only entanglements are probed at these  $Wi$ , as argued above. For  $\tau_H/\lambda > 10$  and low  $Wi$  (regime IV), associations are recovering with increasing  $\tau_H$ . We can clearly see the effect of bond strength on the relative recovery when comparing MEA-UPyMA and nBA-AA. The weaker associations of nBA-AA (despite the much larger number of associations per chain) recover much faster than MEA-UPyMA with regards to the backbone relaxation. This indicates that the time to recovery is more appropriately scaled by some multiple of the bond lifetime which Stukalin et al. argue is the equilibration time  $\tau_{eq}$ .  $\tau_{eq}$  is the timescale for equilibration of unpaired associations within the bulk network and accounts for both the number and strength of stickers as well as the relaxation time of

the monomer.

Figure 10b shows the relative stress recovery as a function of  $\tau_H$  normalized by  $\tau_{eq}$ . This figure clearly shows that the recovery of MEA-UPyMA is probed at very low values of  $\tau_H/\tau_{eq}$  and therefore the recovery is expected to be slow. What is surprising is the very low values of stress recovery for nBA-AA networks. This can be explained by bringing forth arguments from Stukalin et al. where the rate of recovery of bridges strongly depends on the relative  $\tau_W$ . For nBA-AA, the waiting time is such that we are in the “adhesion-hopping regime”, which is the slowest recovery regime. Additionally, Stukalin’s model does not take into account recovery of entanglements which most certainly would slow down recovery. We expect that free associations only become available after some convoluted process that involves bond dissociation and reptation dynamics. Lastly, the argument that high  $Wi$  probes only entanglements is strengthened by this figure, since we do not expect full recovery of associations until some multiple of  $\tau_{eq}$ .

## Conclusions

In this work, we show that measuring and quantifying intrinsic, autonomic self-healing in associating networks is not trivial and depends on experimental conditions and material characteristics. More specifically, self-healing recovery behavior depends on three key timescales: (1) the waiting time before recovery  $\tau_W$ , (2) the time of recovery  $\tau_H$ , and (3) the normalized kinematic flow timescale or  $Wi$ . Using nBA-AA (6%) and MEA-UPyMA (3%), we show that the evolution of recovery as a function of  $\tau_W$  depends on the availability of free associations. When  $\tau_W$  is on the order  $\tau_b$ , both associating polymers show a relatively flat recovery with increasing  $\tau_W$ . Furthermore, for waiting times larger than  $\tau_b$ , the experimental trends show a decreasing recovery due to the internalization of free associating groups. These two findings are in very good agreement with the arguments of Stukalin et al. However, we show for MEA-UPyMA (3%) that the creation of a free surface via cutting leaves behind very

few free associations and thus an increase in recovery is observed until  $\tau_W$  is on the order  $\tau_b$ , which is not captured by the model of Stukalin et al. We argue that this is due to the irreversible damage to chains during the creation of the free surface, not considered in the original model.

For constant  $\tau_W$  and varying  $\tau_H$ , our data and analysis of unentangled, associating polymers validate the healing model presented by Stukalin et al. However the recovery of entangled polymers is not so simple. The entangled polymer first shows recovery of entanglements followed by very slow recovery of associations, indicating a sequential healing process. Furthermore different stress and strain recoveries are observed for the entangled polymer probed at different  $Wi$ . In high  $Wi$  flow, entanglements dominate the measurement, leading to high stress recoveries which remain constant for  $\tau_H/\lambda > 10$ . In low  $Wi$  flow, both entanglement and association recovery is measured. The recovery dynamics of nBA-AA suggest that entanglements play a key role in the timescale for full recovery. This work provides a framework for both self-healing recovery measurements and the development of more complex models.

## References

- (1) Lange, R. F. M.; Van Gurp, M.; Meijer, E. W. *J. Polym. Sci. Part A Polym. Chem.* **1999**, *37*, 3657–3670.
- (2) Folmer, B. B. J. B.; Sijbesma, R. P.; Versteegen, R. M.; Rijt, J. A. J. V. D.; Meijer, E. W. *Adv. Mater.* **2000**, *12*, 874–878.
- (3) Cordier, P.; Tournilhac, F.; Soulie-Ziakovic, C.; Leibler, L. *Nature* **2008**, *451*, 977–980.
- (4) Hentschel, J.; Kushner, A. M.; Ziller, J.; Guan, Z. *Angew. Chemie* **2012**, *124*, 10713–10717.
- (5) Faul, B. C. F. J.; Antonietti, M. *Adv. Mater.* **2003**, *15*, 673–683.
- (6) Aboudzadeh, M. A.; Muñoz, M. E.; Santamaría, A.; Marcilla, R.; Mecerreyes, D. *Macromol. Rapid Commun.* **2012**, *33*, 314–318.
- (7) Yuan, J.; Fang, X.; Zhang, L.; Hong, G.; Lin, Y.; Zheng, Q.; Xu, Y.; Ruan, Y.; Weng, W.; Xia, H.; Chen, G. *J. Mater. Chem.* **2012**, *22*, 11515–11522.
- (8) Bode, S.; Zedler, L.; Schacher, F. H.; Dietzek, B.; Schmitt, M.; Popp, J.; Hager, M. D.; Schubert, U. S. *Adv. Mater.* **2013**, *25*, 1634–1638.
- (9) Burattini, S.; Merino, H.; Weng, W.; Rowan, S. J. *J. Am. Chem. Soc.* **2010**, *132*, 12051–12058.
- (10) Chen, S.; Mahmood, N.; Beiner, M.; Binder, W. H. *Angew. Chemie Int. Ed.* **2015**, *54*, 10188–10192.
- (11) Blaiszik, B. J.; Kramer, S. L. B.; Olugebefola, S. C.; Moore, J. S.; Sottos, N. R.; White, S. *Annu. Rev. Mater. Res.* **2010**, *40*, 179–211.
- (12) Ghosh, S., Ed. *Self-healing Materials: Fundamentals, Design Strategies, and Applications*; Wiley-VCH: Weinheim, Germany, 2009.

- (13) Stukalin, E. B.; Cai, L.; Kumar, N. A.; Leibler, L.; Rubinstein, M. *Macromolecules* **2013**, *46*, 7525–7541.
- (14) Binder, W. H., Ed. *Self-Healing Polymers: from Principles to Applications*; Wiley-VCH: Weinheim, Germany, 2013.
- (15) Herbst, F.; Döhler, D.; Michael, P.; Binder, W. H. *Macromol. Rapid Commun.* **2013**, *34*, 203–220.
- (16) van Gemert, G.; Peeters, J. W.; Söntjens, S. H. M.; Janssen, H. M.; Bosman, A. W. *Macromol. Chem. Phys.* **2012**, *213*, 234–242.
- (17) Peterson, A. M.; Jensen, R. E.; Palmese, G. R. *ACS Appl. Mater. Interfaces* **2010**, *2*, 1141–1149.
- (18) Pratama, P. A.; Peterson, A. M.; Palmese, G. R. *Polym. Chem.* **2013**, *4*, 5000.
- (19) Pratama, P. A.; Shari, M.; Peterson, A. M.; Palmese, G. R. *ACS Appl. Mater. Interfaces* **2013**, *5*, 12425–12431.
- (20) Neuser, S.; Michaud, V. *Exp. Mech.* **2014**, *54*, 293–304.
- (21) Williams, H.; Trask, R.; Knights, A.; Williams, E.; Bond, I. *J. R. Soc. Interface* **2008**, *5*, 735–747.
- (22) Chen, C.; Peters, K.; Li, Y. *Smart Mater. Struct.* **2013**, *22*.
- (23) Pang, J. W.; Bond, I. P. *Compos. Sci. Technol.* **2005**, *65*, 1791–1799.
- (24) Trask, R. S.; Bond, I. P. *Smart Mater. Struct.* **2006**, *15*, 704–710.
- (25) Scheltjens, G.; Diaz, M. M.; Brancart, J.; Van Assche, G.; Van Mele, B. *React. Funct. Polym.* **2013**, *73*, 413–420.
- (26) Zhu, K.; Song, Q.; Chen, H.; Hu, P. *J. Appl. Polym. Sci.* **2018**, *135*, 1–7.

- (27) Baek, P.; Aydemir, N.; Chaudhary, O. J.; Wai Chi Chan, E.; Malmstrom, J.; Giffney, T.; Khadka, R.; Barker, D.; Travas-Sejdic, J. *RSC Adv.* **2016**, *6*, 98466–98474.
- (28) Hsu, H.-r.; Cao, W.; Yang, F.; Lee, S. *J. Polym. Res.* **2017**, *24*, 1–8.
- (29) Shabbir, A.; Goldansaz, H.; Hassager, O.; Ruymbeke, E. V.; Alvarez, N. J. *Macromolecules* **2015**, *48*, 5988–5996.
- (30) Shabbir, A.; Javakhishvili, I.; Cervený, S.; Hvilsted, S.; Skov, A. L.; Hassager, O.; Alvarez, N. J. *Macromolecules* **2016**, *49*, 3899–3910.
- (31) Ahmadi, M.; Hawke, L. G.; Goldansaz, H.; Van Ruymbeke, E. *Macromolecules* **2015**, *48*, 7300–7310.
- (32) Goldansaz, H.; Fustin, C. A.; Wübbenhorst, M.; Van Ruymbeke, E. *Macromolecules* **2016**, *49*, 1890–1902.
- (33) Hawke, L. G. D.; Ahmadi, M.; Goldansaz, H.; van Ruymbeke, E. *J. Rheol.* **2016**, *60*, 297–310.
- (34) Jangizehi, A.; Ghaffarian, S. R.; Schmolke, W.; Seiffert, S. *Macromolecules* **2018**, *51*, 2859–2871.
- (35) Doi, M.; Edwards, S. F. *The Theory of Polymer Dynamics*; Oxford University Press: New York, 1986.
- (36) Rubinstein, M.; Colby, R. H. *Polymer Physics*; Oxford University Press: New York, 2003.
- (37) Roy, D.; Roland, C. M. *Macromolecules* **2013**, *46*, 9403–9408.
- (38) Elliott, B. M.; Steckbeck, K. E.; Murray, L. R.; Erk, K. A. *Int. J. Pharm.* **2013**, *457*, 118–123.

- (39) Thornell, T. L.; Helfrecht, B. A.; Mullen, S. A.; Bawiskar, A.; Erk, K. A. *ACS Macro Lett.* **2014**, *3*, 1069–1073.
- (40) Thornell, T. L.; Subramaniam, K.; Erk, K. A. *J. Polym. Sci. Part B Polym. Phys.* **2016**, *54*, 1693–1701.
- (41) Wang, Y.; He, J.; Aktas, S.; Sukhishvili, S. A.; Kalyon, D. M. *J. Rheol.* **2017**, *61*, 1103–1119.
- (42) Bose, R. K.; Enke, M.; Grande, A. M.; Zechel, S.; Schanher, F. H.; Hager, M. D.; Garcia, S. J.; Schubert, U. S.; van der Zwaag, S. *Eur. Polym. J.* **2017**, *93*, 417–427.
- (43) Yan, T.; Schröter, K.; Herbst, F.; Binder, W. H.; Thurn-Albrecht, T. *Sci. Rep.* **2016**, *6*, 32356.
- (44) Skrzyszewska, P. J.; Sprakel, J.; Wolf, F. A. D.; Fokkink, R.; Stuart, M. A. C.; Gucht, J. V. D. *Macromolecules* **2010**, *43*, 3542–3548.
- (45) Bose, R. K.; Hohlbein, N.; Garcia, S. J.; Schmidt, A. M.; van der Zwaag, S. *Polymer (Guildf)*. **2015**, *69*, 228–232.
- (46) Wubbenhorst, M.; van Turnhout, J.; Folmer, B.; Sijbesma, R.; Meijer, E. *IEEE Trans. Dielectr. Electr. Insul.* **2001**, *8*, 365–372.
- (47) Cate, A. T.; Beek, D. J. M. V.; Spiering, A. J. H.; Dankers, P. Y. W.; Sijbesma, R. P.; Meijer, E. W. *Polym. Prepr.* **2003**, *44*, 618–619.
- (48) Marín, J. M. R.; Huusom, J. K.; Alvarez, N. J.; Huang, Q.; Rasmussen, H. K.; Bach, A.; Skov, A. L.; Hassager, O. *J. Nonnewton. Fluid Mech.* **2013**, *194*, 14–22.
- (49) Alvarez, N. J.; Marin, J. M. R.; Huang, Q.; Michelsen, M. L.; Hassager, O. *Phys. Rev. Lett.* **2013**, *110*, 1–4.

- (50) Bach, A.; Almdal, K.; Rasmussen, H. K.; Hassager, O. *Macromolecules* **2003**, *36*, 5174–5179.
- (51) Ferry, J. D. *Viscoelastic Properties of Polymers*, 3rd ed.; John Wiley & Sons: New York, 1980.
- (52) Münstedt, H. *J. Rheol.* **2014**, *58*, 565–587.
- (53) Morais, M. Quantification of the self-healing behaviour of a supramolecular elastomer by means of peel testing procedure. M.S., Tecnico Lisboa, 2014.
- (54) Li, G.; Meng, H.; Shojaei, A.; Jones, F. R.; Varley, R. J.; Zhu, D. Y.; Rong, M. Z.; Zhang, M. Q. In *Recent Advances in Smart Self-healing Polymers and Composites*; Li, G., Meng, H., Eds.; Woodhead Publishing: Cambridge, UK, 2015.
- (55) Zhong, N.; Post, W. *Compos. Part A Appl. Sci. Manuf.* **2015**, *69*, 226–239.
- (56) Wypych, G. *Self-Healing Materials: Principles and Technology*; ChemTec Publishing: Toronto, 2017.
- (57) Chen, Y.; Kushner, A.; Williams, G.; Guan, Z. *Nat. Chem.* **2012**, *4*, 467–472.
- (58) Wu, D.; Meure, S.; Solomon, D. *Prog. Polym. Sci.* **2008**, *33*, 479–522.
- (59) Willett, J. L.; O'Connor, K. M.; Wool, R. P. *J. Polym. Sci. Part B Polym. Phys.* **1986**, *24*, 2583–2589.
- (60) Plazek, D. J.; Echeverra, I. *J. Rheol.* **2000**, *44*, 831–841.
- (61) Shivokhin, M. E.; Narita, T.; Talini, L.; Habicht, A.; Seiffert, S.; Indei, T.; Schieber, J. D. *J. Rheol.* **2017**, *61*, 1231–1241.
- (62) O'Connor, T. C.; Alvarez, N. J.; Robbins, M. O. *Phys. Rev. Lett.* **2018**, *121*, 47801.

# Table of Contents Figure

